

NASA Technical Memorandum 100738

Flow Fields of Low Pressure Vent Exhausts

John J. Scialdone

July 1989

**(NASA-TM-100738) FLOW FIELDS OF LOW
PRESSURE VENT EXHAUSTS (NASA, Goddard
Space Flight Center) 15 p CSCL 21H**

N89-26902

**Unclas
G3/20 0224111**

The NASA logo, consisting of the word "NASA" in a bold, sans-serif font.

NASA Technical Memorandum 100738

Flow Fields of Low Pressure Vent Exhausts

John J. Scialdone
NASA/ Goddard Space Flight Center
Greenbelt, Maryland

NASA

National Aeronautics and
Space Administration

Goddard Space Flight Center
Greenbelt, Maryland

1989

FLOW FIELDS OF LOW PRESSURE VENT EXHAUSTS

John J. Scialdone

NASA Goddard Space Flight Center, Greenbelt, MD 20771

OVERVIEW

The flow fields produced by low pressure gas vents have been described based on experimental data obtained from tests in a large vacuum chamber. The gas density, pressure, and flux at any location in the flow field are calculated based on the vent plume description and the knowledge of the flow rate and velocity of the venting gas. The same parameters and the column densities along a specified line of sight traversing the plume are also obtained and shown by a computer-generated graphical representation. The fields obtained with a radially scanning Pitot probe within the exhausting gas are described by a power of the cosine function, the mass rate and the distance from the exit port. The field measurements were made for gas at pressures ranging from 2 to 50 torr venting from pipe fittings with diameters of 3/16 inch to 1-1/2 inch I.D. (4.76 mm to 38.1 mm). The N_2 mass flow rates ranged from $2E-4$ to $3.7E-1$ g/s.

Introduction

Many spacecraft and the space station in particular, require venting of gases. The venting may be used to dispose of waste gases, to produce low-pressure drag makeup propulsion, or simply to provide low-level propulsion for attitude control or transfer. Contrary to these benefits, gas ventings in orbit have objectionable effects. The vented gases modify the environment and impact scientific and technical activities. They degrade the thermo-optical properties of surfaces where they may deposit or induce objectionable torque disturbances to the spacecraft. The environment modification may result in gaseous obscuration and molecular scattering in the field of view of an observatory instrument or of an observer. The vented gas deposited on critical surfaces can result in the complete degradation of an instrument or a system. The disturbance torque from a vent may result in a considerable expenditure of spacecraft propulsive power to correct for the unwanted disturbances.

This paper provides experimental data on the flow field produced by the gas vented in a large vacuum chamber from a pipe having inside diameters ranging from 3/16 to 1-1/2 in. The pressure of N_2 in the pipe ranged from 2 to 50 torr and the mass rates from $(2 \times 10^{-4}$ to 3.7×10^{-1} g/s). The flow fields were obtained by measuring the dynamic pressures (ρV^2) radially about the exhaust using a simple Pitot probe. The $\theta_{1/2}$ angle corresponding to 50 percent of the maximum Pitot pressures at the vent centerline was used with other parameters to provide an analytical description of the plume.

The characterization of the plumes and a knowledge of the vent gas terminal velocity allows, as shown, an estimate of the flux, the density, and the pressure at various locations in the plume flow field including surfaces where contamination may occur as a result of plume impingement. It provides for the evaluation of the column density along a line of sight traversing the plume, and for estimation of the return flux from the self scattering of the gas within the plume and with the ambient residual atmosphere. Also, the flow field description provides the definition of the gas propulsive thrust vector.

The paper indicates the techniques employed for the plume description, the measurements made, the parameters affecting the plume, and the analysis for the implementation of the results in a form which can be used for other plume conditions. A computer program has been written to plot in a normalized format the plume flux contours which also represent the density and pressure contours. The inclusion of these plots of a line describing an observation line of sight crossing the plume provides gaseous parameters of interest along that line and the evaluation of the column density.

The experimental investigation described here was carried out several years ago as the basis for a space experiment. The experiment described in Reference (1) measured the return flux scattered by the ambient atmosphere of a source of gas (neon) ejected on command from the spacecraft. The data reported here were needed to obtain an analytical description

of the emitted neon plume. The investigation sought to produce a plume having a Lambertian distribution, which would offer a sufficient ambient scattering cross section for the return flux and, at the same time, provide a very low thrust and a low exhaust mass rate.

Experimental Procedures

The radial distribution of the gas flow vented from pipes of various diameters and for various mass flows was measured in a large vacuum chamber (3.65 m diameter, 4.57 m high) using the arrangement shown in Figure 1. A variable-size gas fitting was fitted to a 92-cm long, 4.76-mm I.D. Teflon tube. A Baratron^(R) capacitance pressure manometer, which when properly calibrated and temperature-controlled, can measure pressures down to 10^{-5} torr, was connected to the other end of the Teflon tube. The reference pressure of the Baratron was the chamber pressure. A sintered flow restrictor was located approximately 12 cm upstream of the pressure-measuring Baratron. The restrictor provided a neon flow of 4333 std cm^3/min at 525 psig supply pressure and conductance of about $1.96 cm^3$, as determined from previous independent tests. The same restrictor, as will be shown, provided a nitrogen flow of 79 percent that of the neon, or 3440 std cm^3/min .

A pressure gage, a pressure regulator, and the supply of N_2 were located upstream of the restrictor outside the vacuum chamber. The rate of gas exhausted from the pipe was known from other tests as a function of the supply pressure upstream of the porous plug restrictor and as a function of the supply pressure depletion time as shown in Figure 2. Also, the pressure (P_u), downstream of the plug, was recorded as a function of the supply pressure (P_s) with and without a flow diffuser at the end of the Teflon tube (Figure 3). The diffuser, with a conductance greater than 5 l/s was to provide a spread out of the flow at the exit. The exit venting port at the end of the Teflon tubing, as shown in Figure 1, was firmly held at the centerline, some measured distance away, of a wheel which could be rotated from the outside of the vacuum chamber. The wheel had a slot for the mounting of a bracket holding a fitting attached at the extremity of a flexible tube connected to one of the sides of a Baratron capacitance manometer mounted outside the chamber. The other side of the Baratron was connected to the chamber pressure.

The slot in the rotatable wheel provided for changing the distance between the flow exhaust port and the fitting. The fitting, as a Pitot tube entrance, recorded the dynamic pressure in the gas stream (ρV^2) ($dyne/cm^2$). The Pitot tube fitting was precisely aligned with the centerline of the exhaust vent fitting. The wheel angular motion, and hence, the angular position of the Pitot detector with respect to the centerline of the flow, was measured by a goniometric scale attached to the wheel crank, outside the chamber. Any angular positions could be held indefinitely for measurements under steady flow conditions. The 12-foot (3.65-m)

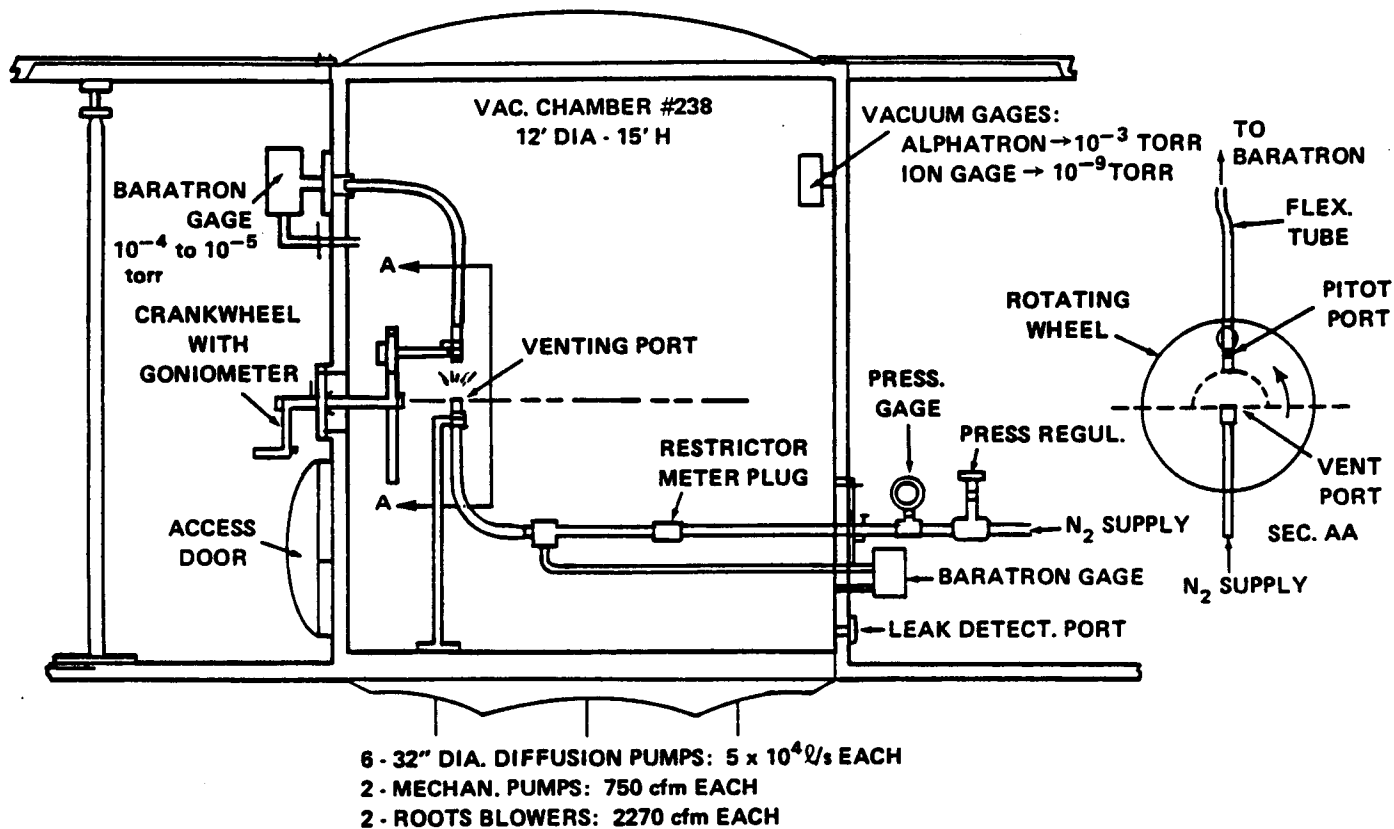


Figure 1. Vacuum system and test arrangement for vent plume flow field description.

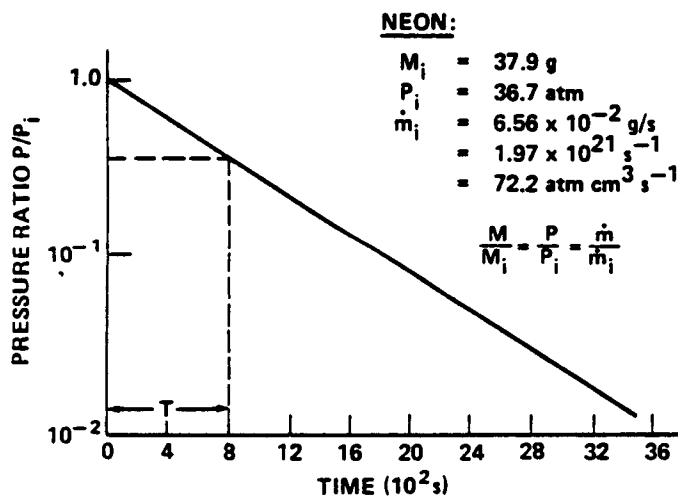


Figure 2. Neon pressure, mass, and flow rate versus time.

diameter by 15-foot (4.57-m) high vacuum chamber was provided with 6 32-inch diameter diffusion pumps, each having 5×10^4 l/s pumping speed, 2 mechanical pumps, and 2 roots blowers. The pumping system was capable of maintaining chamber pressures lower than 10^{-7} torr. The chamber pressure was measured with an Alphasatron gage down to a pressure of 10^{-3} and below this pressure with an ion gage. During the test, with the N_2 being vented in the chamber,

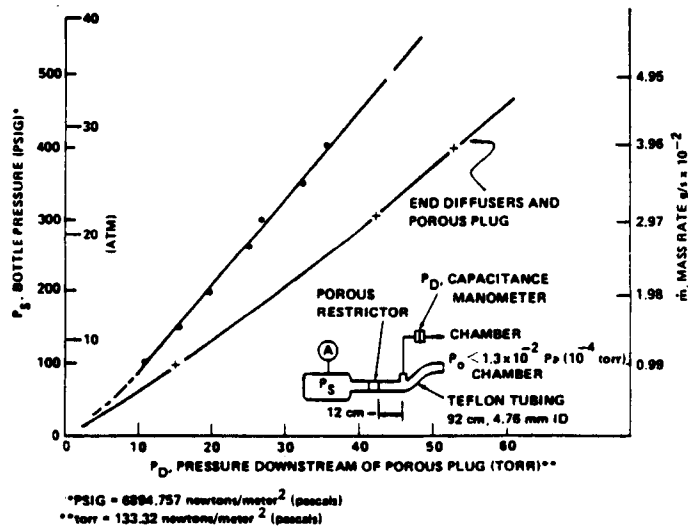


Figure 3. N_2 Downstream pressures and mass rates versus reservoir pressures.

the pressure was, in general, in the 10^{-4} torr range; i.e., about 5 to 6 orders of magnitude lower than the pressure (2 to 50 torr) downstream of the restrictor, and upstream of the gas exit.

The pressure data were collected manually for rotation steps of 5° and 10° , turning the Pitot detector both clockwise and counterclockwise starting with the 0° angle cor-

responding to the aligned detector and venting gas outlet. Measurements were not carried out, in general, beyond 90° from the centerline. At that time, and for the purpose of the test investigation, there was no interest in the backflow (> 90°) measurements. Backflow measurements would have provided flow directed toward the rear of the exhaust vent and would have included measurements beyond the Prandtl-Mayer angles. However, there were occasions when some measurements were made beyond 90°. On those occasions, and in some of those instances, negative pressures (chamber pressures higher than the flow pressure) were noted. This may have been indicative of gas flow creating a venturi effect at the detector entrance.

Several tests were carried out with the detector at various distances from the exit vent. But the majority and most conclusive tests were carried out with the detector 5.1 cm away from the vent exit. The detector tubing was also varied using either a 3/8-inch or a 1/8-inch internal diameter (9.52 mm or 3.17 mm).

Test Parameters

Flow Rate—The nitrogen flow rate was obtained from the appropriate modification of the flow rate found experimentally for the neon. The N_e rate as dictated by the porous restrictor plug was measured to be $Q = 4333 \text{ atm cm}^3/\text{min}$ ($72.21 \text{ cm}^3/\text{s}$) (54.88 torr l/s) when the pressure upstream of the restriction was 525 psig (36.73 atm). The corresponding conductance was $1.96 \text{ cm}^3/\text{s}$. The mass flow rate at standard condition was $\dot{m} = 6.44 \times 10^{-2} \text{ g/s}$ and the molecular flow rate was $n = 1.94 \text{ E}21 \text{ molec/s}$. The flow at the restrictor was sonic or choked since the downstream pressures were always $P_D \ll P_S$.

The equivalent N_2 -choked flow accounting for the difference in molecular masses and specific heat ratio can be evaluated from Reference 2,

$$\frac{Q_{N_2}}{Q_{N_e}} = \left(\frac{M_{N_2}}{M_{N_e}} \right)^{1/2} \frac{\left[\gamma \left(\frac{2}{\gamma+1} \right)^{\frac{\gamma+1}{\gamma-1}} \right]_{N_2}}{\left[\gamma \left(\frac{2}{\gamma+1} \right)^{\frac{\gamma+1}{\gamma-1}} \right]_{N_e}} = 0.84 \left(\frac{0.6839}{0.725} \right) = 0.794 \quad (1)$$

where $M_{N_2} = 20 \text{ g/mole}$, $M_{N_2} = 28 \text{ g/mole}$, $\gamma_{N_2} = 1.66$, $\gamma_{N_2} = 1.4$.

The N_2 flow rate is then $57.33 \text{ atm cm}^3/\text{s}$ (5.2 E-2 g/s ; 1.56 E-21 s^{-1}) for a supply pressure of 525 psi and the restrictor conductance is $1.55 \text{ cm}^3/\text{s}$.

Pressure Downstream of the Restrictor, Upstream of the Exit—The pressure downstream of the restrictor as a function of the restrictor upstream pressure was measured in a vacuum chamber and is reported in Figure 3. The measurements

were made with a capacitance manometer using the vacuum chamber pressure as a reference pressure. The pressure was measured at about 12 cm downstream of the restrictor and about 80 cm from the end of the Teflon tubing. The long length of tubing was made necessary by installation requirements for the neon supply reservoir location aboard the spacecraft.

The N_2 mass flow rate is shown on the same plot in terms of the supply pressure. The plot also included the downstream pressure when a diffuser was added at the end of the tubing. That diffuser had a conductance much greater than that of the restrictor plug. It was employed to spread out the flow at the exit of the tubing. It did not, however, provide the intended function.

Exit Flow Velocities—A choked critical velocity exists at the tubing exit when the downstream to the exit pressure for N_2 is $P_c < .53 P_D$. The pressure P_D , as shown, varied from about 50 torr down to 1 or 2 torr, while the chamber pressure (P_c) was always several orders of magnitude lower than that. The critical velocity for the N_2 at $T = 290 \text{ K}$ can be calculated as:

$$V_c = \left(\frac{2\gamma}{\gamma+1} \frac{RT}{M} \right)^{1/2} = 316 \text{ m/s} \quad (2)$$

where $\gamma = 1.4$, $M = 28$, and $R = 8.31 \times 10^7 \text{ erg/mole K}$ is the gas constant. The terminal velocity reached downstream of the exit port, for an adiabatic isentropic expansion, is

$$V_T = \left(\frac{2\gamma}{\gamma-1} \frac{RT}{M} \right)^{1/2} = 725 \text{ m/s.} \quad (3)$$

The Mach number based on the critical velocity is $M = (V_T)/(V_c) = 2.44$ at the terminal velocity. The temperature at this Mach number is

$$T = T_o \left(1 + \frac{\gamma-1}{2} M^2 \right)^{-1} = 132 \text{ K.} \quad (4)$$

The distance Z downstream of the exit port of diameter D where the maximum adiabatic terminal velocity has been established, can be estimated based on an approximate relationship valid for $Z/D \gg 1$ and $\rho/\rho_s \ll 1$, Refs. 3, 4, 5, 6.

$$M = \left(\frac{\gamma+1}{\gamma-1} \right)^{1/4} \left(\frac{Z}{D} \right)^{\gamma-1} \quad (5)$$

which for the value of $M = 2.44$ indicates that $Z \sim 0.63D$. This indicates that at the distance of 5.1 cm (or 6.8 cm) used in the present tests for the location of the Pitot tube, the flow would have reached maximum velocity.

Exhaust Exit Ports—The exhaust port provided by pipe fittings, varied from 3/16 inch (0.476 cm) to 1-1/2 inches (3.18 cm) internal diameter. The diffuser had a centered exit area

corresponding to 7/8 inch (2.23 cm) in diameter. For all tests, with the exception of one, the length of the pipe fittings to their internal diameters (L/D) were much greater than one.

Test Data

The experimental flow fields measured for various vent sizes and vent pressures are shown in Figures 4 through 10. The vent upstream pressures varied from about 2 to 50 torr and the downstream chamber pressures ranged down to 10^{-4} torr during the measurements. The mass flow rates were from 3.7×10^{-1} to 2×10^{-4} g/s. For some initial measurements carried out in a small vacuum chamber and reported here for completeness, the chamber pressures ranged from 10^{-3} to 10^{-1} torr. The various parameters for the test conditions are indicated on the plots. The plots also indicate the value of angle $\theta_{1/2}$. This is the angle corresponding to the Pitot measurement pressure value of 1/2 the maximum pressure measured at the centerline of the flow. The magnitude of that angle is a measure of the plume spread. For the present test parameters, the $\theta_{1/2}$ angle varied from an aver-

age value of 48 degrees when the pressures in the chamber were in the 10^{-4} torr range and average values of 18 to 20 degrees when those pressures were in the 10^{-1} torr range. Flow field results with the high chamber background pressures using 1/4-, 3/8-, and 3/4-inch (6.25, 9.52 and 19.05 mm) diameter exhaust pipe openings and for a 0.196-in. (0.498-mm) diameter, 0.029-inch (0.736-mm) thickness orifice, are also being reported. These results were obtained when the downstream chamber pressures were in the 10^{-3} torr range or higher. The lowest upstream pressure was 2 torr which resulted in a 3- to 4-order-of-magnitude-difference between upstream and downstream pressures.

Data Reduction and Application

The normalized Pitot pressures versus angles obtained from the tests, when superimposed on a graph (Figure 11) showing the function of $\cos^n \theta$ for values of n from 1 to 5, show that the pressures can be represented for a considerable range of angles (from 0° to $75-80^\circ$) quite well by a cosine power function. The data obtained for the 3/16-inch (4.76-mm) diameter pipe, $P_u = 25.3$ torr, $P_c = 6.3 \times 10^{-4}$ torr, $\theta_{1/2} = 48^\circ$, and for those of the 1-1/2-inch (38.1-mm) diameter pipe, $P_u = 37$, $P_c = 9.3 \times 10^{-4}$, $\theta_{1/2} = 40^\circ$, have been superimposed on the cosine plots. The divergence occurs beyond $75-80^\circ$ where the data obtained from the measurements is not available, or careful measurements were not taken, at those angles. The Pitot pressures for those large angles were less than 5 percent of the maximum ΔP pressure at the centerline.

The fraction of gas included at those angles is about 2 percent of the total, and in those regions, the plumes may be represented by an exponential function. This was not done because of the limited data available.

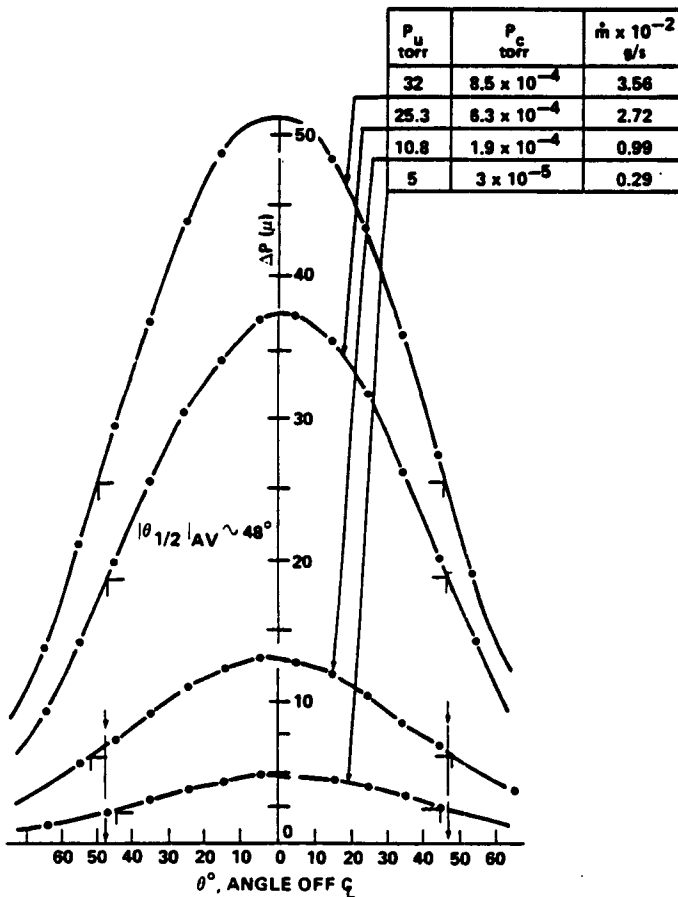


Figure 4. Pitot pressures as a function of angles off ζ . Pitot opening dia., $d = 3/8$ in; radial distance of Pitot, $r = 5.1$ cm; pipe exit I.D. = 3/16 in. (4.76 mm).

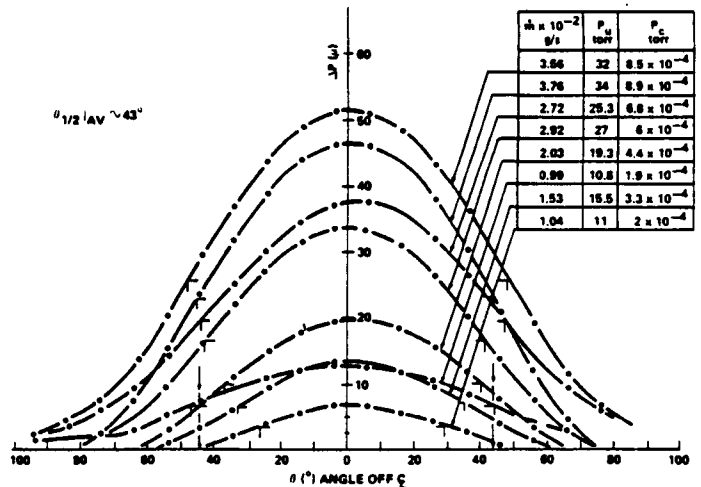


Figure 5. Pitot pressures as a function of angles off ζ of pipe flow. Pitot opening dia., $d = 1/8$ in.; radial distance of Pitot, $r = 5.1$ cm; pipe exit I.D. = 3/16 in. (4.76 mm).

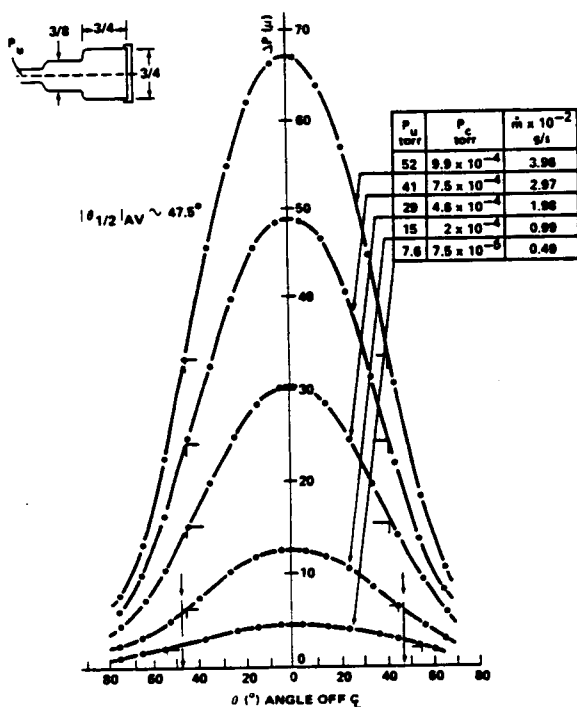


Figure 6. Pitot pressures as a function of angles off \mathcal{C} of pipe flow. Pitot opening dia., $d = 1/8$ in.; radial distance of Pitot, $r = 5.1$ cm; pipe exit I.D. = $3/4$ in. (1.90 cm).

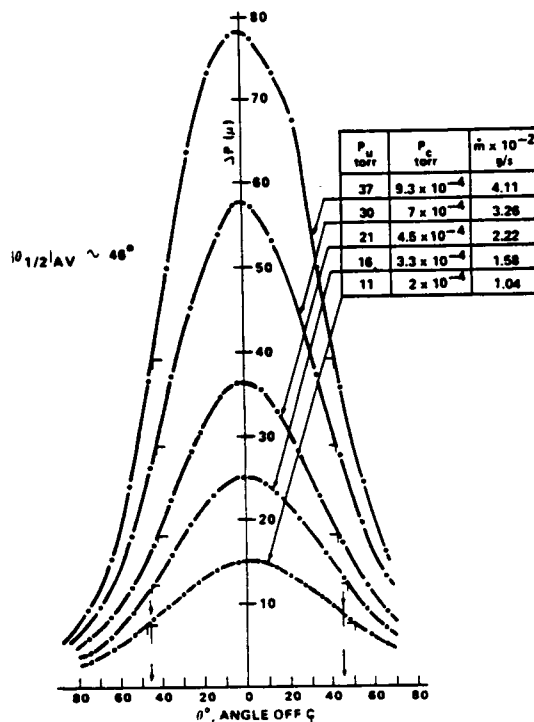


Figure 8. Pitot pressure as a function of angles off \mathcal{C} of pipe flow. Pitot opening dia., $d = 3/8$ in.; radial distance of Pitot, $r = 5.1$ cm; pipe exit I.D. = 1 in. (2.54 cm).

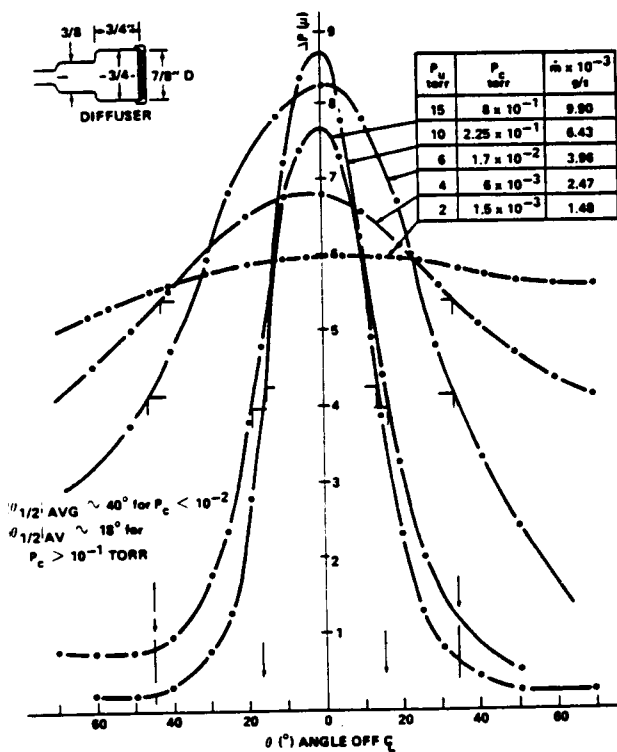


Figure 7. Pitot pressures as a function of angles off \mathcal{C} of pipe flow. Pitot opening dia., $d = 1/8$ in.; radial distance of Pitot, $r = 5.1$ cm; diffuser $7/8$ in. dia (2.22 cm).

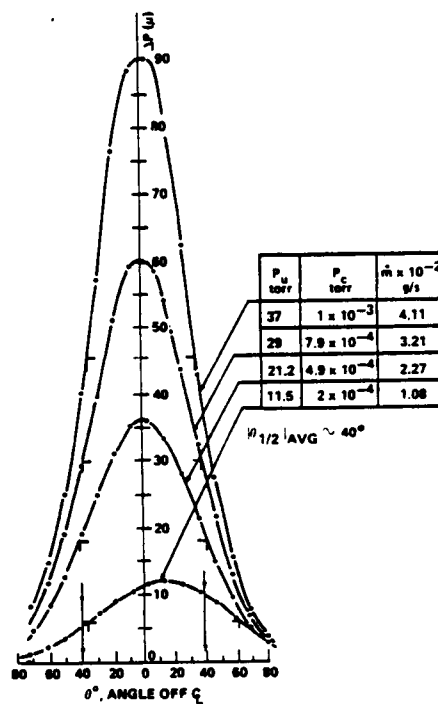


Figure 9. Pitot pressure as a function of angles off \mathcal{C} of pipe flow. Pitot opening dia., $d = 1/8$ in.; radial distance, $r = 5.1$ cm.; pipe exit I.D. = 1.5 in. (3.81 cm).

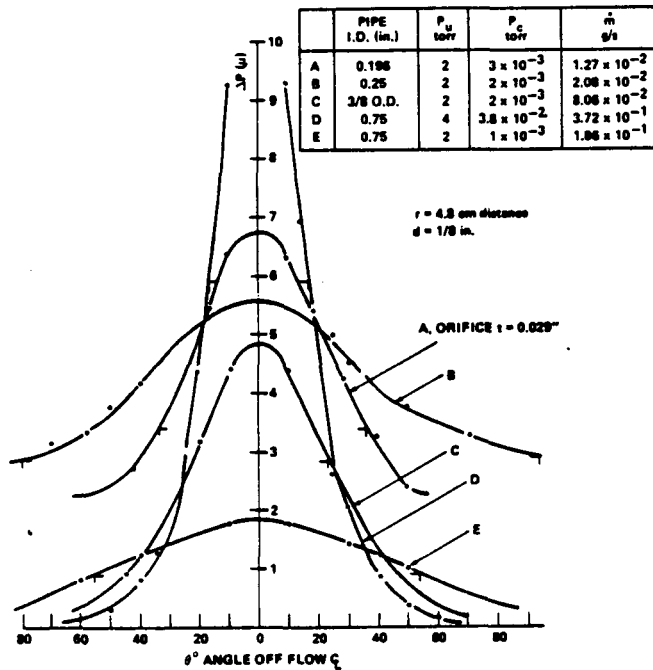


Figure 10. Pitot pressures as a function of angles off \mathcal{Q} of pipe flow.

The value of the exponent of the cosine function appropriate for each distribution can be obtained as shown in Figure 12 by plotting on log paper $\cos^n \theta$ versus the normalized Pitot pressure, $\Delta P/\Delta P_{\max}$. The slope of the curve provides the value of n . The straight lines were drawn attempting a best fit. It is apparent that the experimental data fit the straight line reasonably well with the divergence occurring at the large angles. The $\theta_{1/2}$ angle from these plots is seen to become smaller as the size of the vent grows from 3/16 inch to 1-1/2 inch (4.76 mm to 38.1 mm). The exponent of the cosine grows from about $n = 1.74$ to $n = 2.51$. It is, therefore, reasonable to use a cosine function to represent the plumes investigated here. However, one should be aware that at large angles, an error is being introduced.

The flux of gas ϕ ($\text{g cm}^{-2} \text{ s}^{-1}$; $\text{cm}^{-2} \text{ s}^{-1}$) exhausting from one of the above openings can be represented, based on the above discussion, by $\phi = k \cos^n \theta$ where k is a constant to be determined. The elemental mass of gas $d\dot{m}$ in traversing an element area of dA of an axisymmetrical plume will be ϕdA and the total mass rate will be

$$\dot{m} = \int_A \phi dA.$$

The element of area using polar coordinates is

$$dA = r d\theta (r \sin\theta d\varphi) = r^2 \sin\theta d\theta d\varphi$$

where $0 < \theta < \pi/2$ is the angle of the centerline of the plume to the element of area, $0 < \varphi < 2\pi$ is the angle of symmetry,

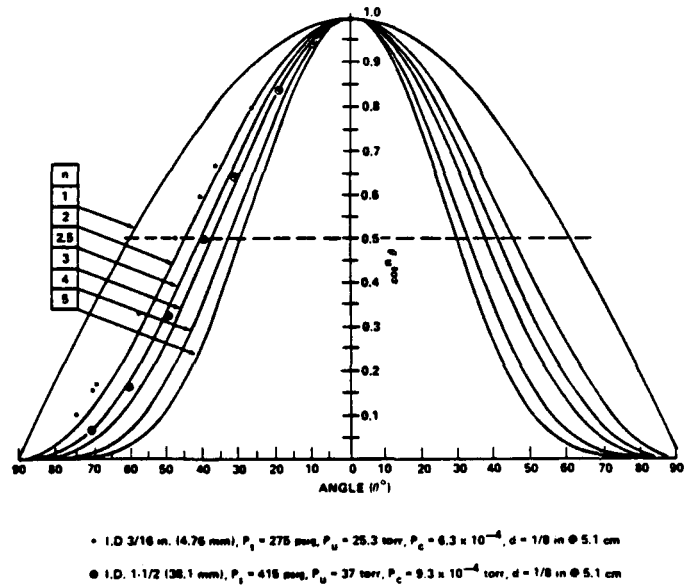


Figure 11. $\cos^n \theta$ versus θ .

and r is the distance from the center of the source at the exit to the element of area.

The integration giving the total flow rate is then

$$\begin{aligned} \dot{m} &= \int_A \phi dA = k \int_A \cos^n \theta (r^2 \sin\theta d\theta d\varphi) = \\ &= k \int_0^{2\pi} r^2 d\varphi \int_0^{\pi/2} \cos^n \theta \sin\theta d\theta = \\ &= k \left[2\pi r^2 \left(-\frac{\cos^{n+1}\theta}{n+1} \right) \right]_0^{\pi/2} = \frac{2\pi r^2}{n+1} k \end{aligned}$$

and the constant is $k = \dot{m} \left(\frac{n+1}{2\pi r^2} \right)$. (6)

The flux at a distance r and angle θ from the centerline is given in terms of the total mass rate being exhausted

$$\phi = \frac{n+1}{2\pi r^2} \dot{m} \cos^n \theta \quad (\text{g cm}^{-2} \text{ s}^{-1}; \text{cm}^{-2} \text{ s}^{-1}; \text{moles s}^{-1} \text{ cm}^{-2})$$
 (7)

where the units of the flux depend on the units of \dot{m} and r .

Application

The expression for the flux also indicates the density at any distance r and angle θ , if the velocity of the flux is known. This density, since $\rho = \phi/V$, is

$$\rho = \left(\frac{n+1}{2\pi r^2} \right) \frac{\dot{m}}{V} \cos^n \theta \quad (\text{g cm}^{-3}; \text{cm}^{-3})$$
 (8)

The pressure, $P = \rho KT = \rho (RT)/(M)$ for a temperature T (K), molecular mass M (gr/mole), and $R = 62.36 \times 10^3$ torr $\text{cm}^3/\text{mole K}$ the gas constant is,

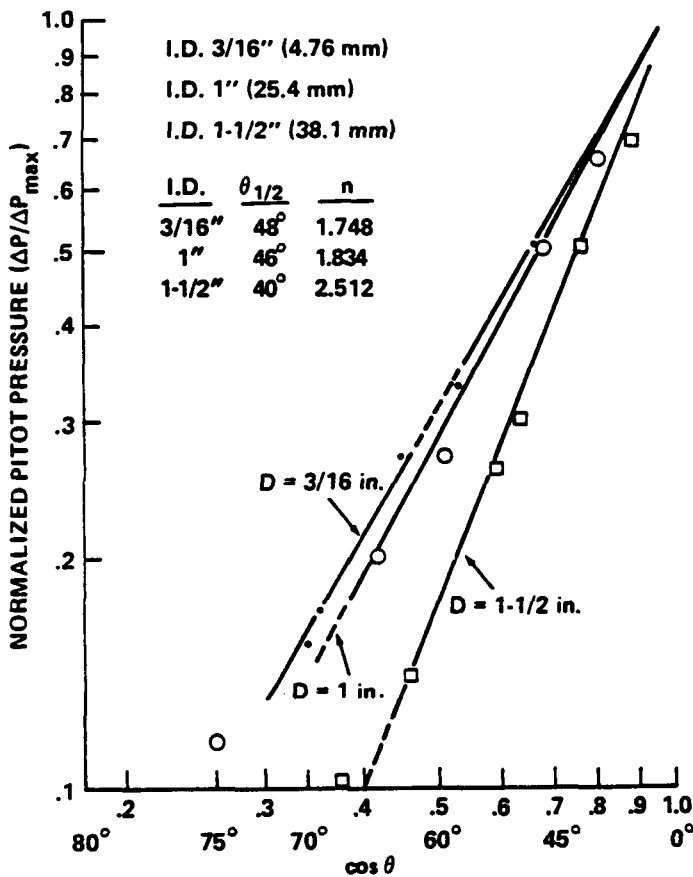


Figure 12. Normalized pressure vs. $\cos \theta$.

$$P = \left(\frac{n+1}{2\pi r^2} \right) \frac{\dot{m}}{V} \frac{RT}{M} \cos^n \theta \quad (\text{torr}) \quad (9)$$

Given then the experimental data on the flow field or simply the angle $\theta_{1/2}$, the mass flow rate \dot{m} , the temperature and the terminal velocity one can estimate pressure, density, and flux at any location within the hemisphere of the gas discharge. These parameters are important for the assessment of contamination hazards to systems exposed to the vented gases, and for an estimate of either the mass or the number column density along a line of sight. The column density is obtained by performing the integration

$$N = \int_0^x \rho dx = \int_0^x \frac{n+1}{2\pi x^2} \frac{\dot{m}}{V} \cos^n \theta dx \quad (10)$$

where x is the distance along the line of sight. By an appropriate description of the line of sight, e.g., by a line $y = ax + b$ described by its angle and origin with respect to the gas source, one can obtain the parameters of interest as the line of sight intersects the plume.

Two computer programs have been written to provide graphically and numerically, those parameters. One needs to input ϕ/\dot{m} values and n for the plume description; the parameters a and b for the equation describing the line of sight; m

(meters), the distance along the line of sight; and the increment of dm (meters) sought for the integration and evaluation of the column density. An example of the plots provided by these programs is shown in Figure 13. For generality, the fluxes as a function of the distances are reported in terms of ϕ/\dot{m} (cm^{-2}) as is the sum of the flux contributions,

$$\sum_0^d \frac{\phi}{\dot{m}} d \quad (\text{cm}^{-2} \text{m})$$

along the LOS. With the exhaust rate \dot{m} , and V the exhaust velocity, one can obtain the flux and the column density, N

$$N = \int_0^d \frac{\phi}{\dot{m}} \frac{\dot{m}}{V} d \quad (\text{g/cm}^2, \text{cm}^{-2}) \quad (11)$$

Similarly, the pressure can be obtained in the same manner using the appropriate expressions.

Conclusions

The radial and angular distribution of the gas flow from openings with large L/D , and diameters ranging from 3/16 inch to 1-1/2 inches (4.76 mm to 38.1 mm) were measured in a large chamber where the pressure was maintained in the 10^{-4} torr range, or lower. The N_2 flow ranged from 2×10^{-4} gr/s to 3.7×10^{-1} gr/s and the pressures upstream of the exhaust vent ranged from 2 torr to 52 torr. Some preliminary tests were carried out in a small chamber. In those tests, the chamber pressures varied from 10^{-1} torr to 10^{-3} torr. A Pitot probe was used to measure the flow rate momentum at various angles from the centerline of the exhaust flow.

The diameter of the Pitot tube opening and its distance from the exhaust aperture were also changed in two instances to evaluate their effects.

The measurements indicated that for the range of upstream pressures and mass flows employed in these tests, the chamber downstream pressure must be about 5 orders of magnitude lower than the pressures at the exhaust. Under those conditions one obtains full lateral expansion of the plume.

The angle, $\theta_{1/2}$, corresponding to 50 percent of the maximum pressure in the flow field at centerline, varies from 40° to 48° when the pressure upstream of the exhaust varies from 2 torr to 50 torr and the chamber pressure is about 4×10^{-4} torr, or lower.

The half angle increases as the pipe opening diameter decreases.

The effect of the downstream pressure severely restricts the spreading of the plume.

The diameter of the Pitot detector was varied from 1/8 inch to 3/8 inch (3.17 mm to 9.52 mm). The change did not affect the measurements. The measurements at each angle from the plume centerline were made by holding the angular positions for a sufficient length of time to insure steady pressure flow conditions at those locations.

The distance of the Pitot detector (5.1 cm or 6.8 cm) did

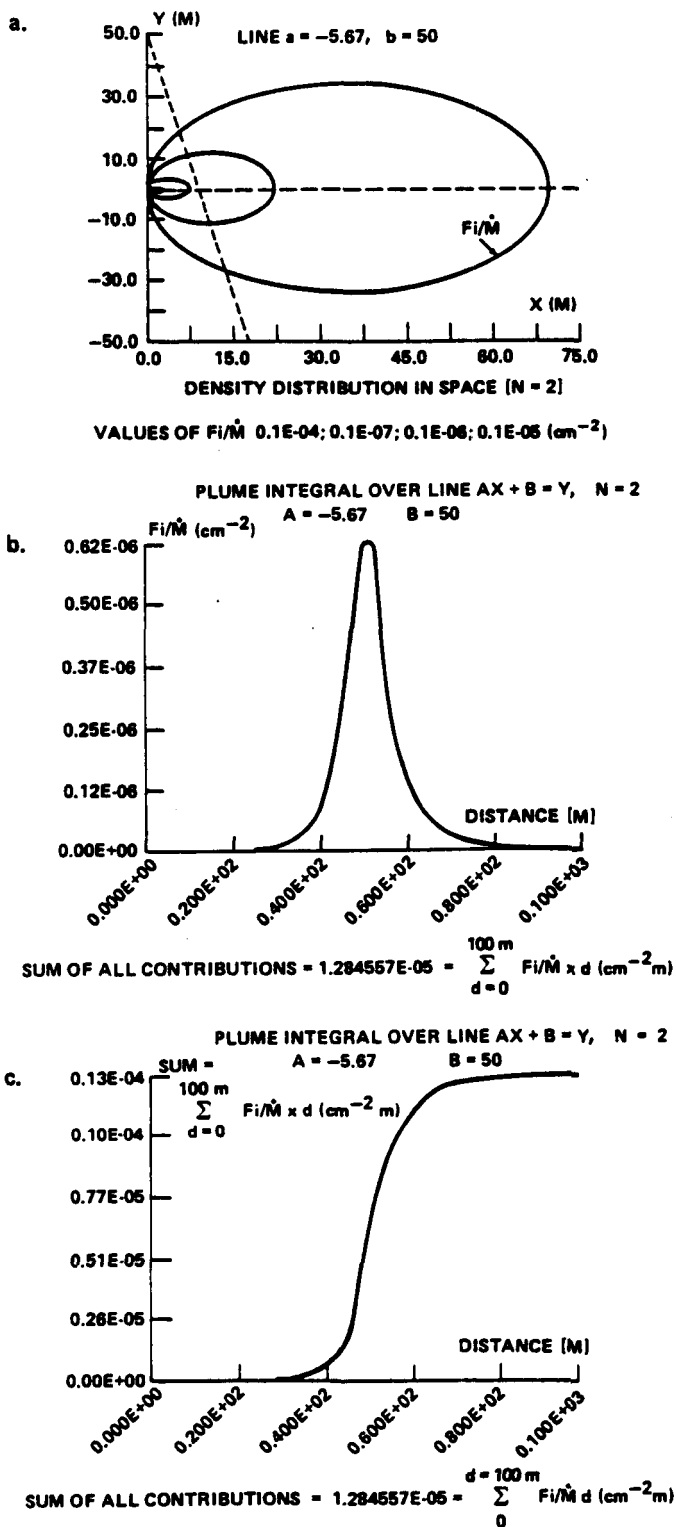


Figure 13. Flux density contours, flux density along a line of sight, and sum of flux density along the line for an N = 2 plume.

not affect the flow distribution. This indicates that the flow was frozen at those distances. The magnitude of the pressure readings decreased with the square of the distance.

Most of the flow patterns were obtained with the detector located 5.1 cm from the exit port. This corresponded to a downstream distance of about 10 diameters for 0.476-cm diameter pipe and 1.33 diameters for the 3.81-cm diameter port.

Measurements beyond 80° were not available because of the limitation in the pressure readings and the lack of interest at those large angles at the time the measurements were made. However, more than 95 percent of the plume mass is contained within the half angles of 75° and about 75 percent of the same mass is within the half angle of 40° .

The flux at the distance r and angle θ from the centerline can be described by a power of the cosine function up to a half angle of about 75° . The flux beyond those angles may be described by an exponential function. This, however, was not attempted. If one chooses to describe the plume with a cosine function up to 90° half angle, the error is then less than 10 percent.

The coefficient in the expression of the cosine function for the plume description includes the mass rate from the vent, the distance at which the flux is being measured, and a factor which includes the power of the cosine function; i.e.,

$$\phi = \frac{n+1}{2\pi r^2} \dot{m} \cos^n \theta.$$

The power of the cosine function can be obtained by plotting on log coordinates the normalized Pitot pressures versus the cosine of the angle. The power can also be obtained by establishing the angle from the centerline where the Pitot pressure is 50 percent of the maximum pressure corresponding to the 0° angle. That value reported on a graph of the cosine to various powers of cosine, can provide the power of n by comparison.

The plume description with the appropriate equation can provide the densities, pressures, and fluxes at any distance and angle from the exhaust aperture within the hemisphere in which the gas is exhausted. Also, one can obtain the same parameters along a line of sight traversing the plume at any angle and originating at a plane parallel to the aperture. The data provide simultaneously the column density which is an important parameter in scientific measurements.

Acknowledgement

The author thanks R. Kruger and B. Paxson for their assistance in setting up and running the tests, and E. Detoma for co-authoring the computer program.

References

1. Scialdone, J.J., "Correlation of Self-Contamination Experiments in Orbit and Scattering Return Flux Calculation," NASA TN-D-8438, March 1977.
2. Santeler, D.J. et al., "Vacuum Technology and Space Simulation," NASA SP-105, 1966, page 92.
3. Fite, W.L., "Expansion of Gases from Molecular Beam Sources," Research Note #1, January 1971, Extranuclear Laboratory, Inc., Pittsburgh, PA.
4. Ashkenas, H., and F.S. Sherman, "The Structure and Utilization of Supersonic Free Jets in Low Density Wind Tunnels," in Rarefied Gas Dynamics, 4th International Symposium, Vol. II, Edited by J.H. deLeeuw, 196, page 84.
5. Anderson, J.B. et al., "Studies of Low Density Supersonic Jet," in Rarefied Gas Dynamics, 4th International Symposium, Vol. II, edited by J.H. deLeeuw, 1966, page 106.
6. French, J.B., "Molecular Beams for Rarefied Gas Dynamics Research," NATO Advisory Group for Aerospace Research and Development, Agardograph 112.



Report Documentation Page

1. Report No. NASA TM-100738	2. Government Accession No.	3. Recipient's Catalog No.	
4. Title and Subtitle Flow Fields of Low Pressure Vent Exhausts		5. Report Date July 1989	
		6. Performing Organization Code 313.0	
7. Author(s) John J. Scialdone		8. Performing Organization Report No. 89B00151	
		10. Work Unit No. n/a	
9. Performing Organization Name and Address Goddard Space Flight Center Greenbelt, Maryland 20771		11. Contract or Grant No.	
		13. Type of Report and Period Covered Technical Memorandum	
12. Sponsoring Agency Name and Address National Aeronautics and Space Administration Washington, D.C. 20546-0001		14. Sponsoring Agency Code	
		15. Supplementary Notes	
16. Abstract The flow fields produced by low pressure gas vents are described based on experimental data obtained from tests in a large vacuum chamber. The gas density, pressure, and flux at any location in the flow field are calculated based on the vent plume description and the knowledge of the flow rate and velocity of the venting gas. The same parameters and the column densities along a specified line of sight traversing the plume are also obtained and shown by a computer-generated graphical representation. The fields obtained with a radially scanning Pitot probe within the exhausting gas are described by a power of the cosine function, the mass rate and the distance from the exit port. The field measurements were made for gas at pressures ranging from 2 to 50 torr venting from pipe fittings with diameters of 3/16 inch to 1-1/2 inches I.D. (4.76 mm to 38.1 mm). The N ₂ mass flow rates ranged from 2E-4 to 3.7E-1 g/s.			
17. Key Words (Suggested by Author(s)) Plumes, Plume Contamination, Auxiliary Propulsion, Vents, Low Pressure Thrusters, Plume Impact, Pipe, Orifice Vent Flow		18. Distribution Statement Unclassified - Unlimited Subject Category 20	
19. Security Classif. (of this report) Unclassified	20. Security Classif. (of this page) Unclassified	21. No. of pages	22. Price